

Interaction of Solitary Waves with a Phase Shift in a Nonlinear Dirac Model

Sihong Shao and Huazhong Tang*

LMAM and School of Mathematical Sciences, Peking University, Beijing 100871, China.

Received 15 May 2007; Accepted (in revised version) 21 August 2007

Available online 18 December 2007

Abstract. This paper presents a further numerical study of the interaction dynamics for solitary waves in a nonlinear Dirac model with scalar self-interaction, the Soler model, by using a fourth order accurate Runge-Kutta discontinuous Galerkin method. The phase plane method is employed for the first time to analyze the interaction of Dirac solitary waves and reveals that the relative phase of those waves may vary with the interaction. In general, the interaction of Dirac solitary waves depends on the initial phase shift. If two equal solitary waves are in-phase or out-of-phase initially, so are they during the interaction; if the initial phase shift is far away from 0 and π , the relative phase begins to periodically evolve after a finite time. In the interaction of out-of-phase Dirac solitary waves, we can observe: (a) full repulsion in binary and ternary collisions, depending on the distance between initial waves; (b) repulsing first, attracting afterwards, and then collapse in binary and ternary collisions of initially resting two-humped waves; (c) one-overlap interaction and two-overlap interaction in ternary collisions of initially resting waves.

AMS subject classifications: 65M60, 35L60, 81Q05

Key words: Discontinuous Galerkin method, phase plane method, Dirac field, Soler model, solitary waves, phase shift.

1 Introduction

Ever since its invention in 1929 the Dirac equation has played a fundamental role in various areas of modern physics and mathematics, and is important for the description of interacting particles and fields. Soler [20] first proposed a classical spinorial model with scalar self-interaction for extended particles by means of nonlinear Dirac (NLD)

*Corresponding author. *Email addresses:* shaosihong@gmail.com (S. H. Shao), hztang@math.pku.edu.cn (H. Z. Tang)

fields. His model is described by the Lagrangian density $L = i\bar{\psi}\gamma^\mu\partial_\mu\psi - m\bar{\psi}\psi + \lambda(\bar{\psi}\psi)^2$, from which we may derive the nonlinear Dirac equation

$$i\gamma^\mu\partial_\mu\psi - m\psi + 2\lambda(\bar{\psi}\psi)\psi = 0, \quad (1.1)$$

where the γ^μ matrices are defined by

$$\gamma^0 = \begin{pmatrix} I & 0 \\ 0 & -I \end{pmatrix}, \gamma^k = \begin{pmatrix} 0 & \sigma^k \\ -\sigma^k & 0 \end{pmatrix},$$

here σ^k with $k=1,2,3$, denote the Pauli matrices. The nonlinear self-coupling term $(\bar{\psi}\psi)^2$ in the Lagrangian allows the existence of finite energy, localized solitary waves, or extended particle-like solutions, see e.g. [20]. Several authors have committed themselves to analytically investigating the Soler model, including stability [2,5–8,21], coupling with other fields [15,16], and some mathematical properties [13]. A review on the Soler model can be found in [14].

The current work is concerned with the numerical investigation of the interaction dynamics of Dirac solitary waves in the Soler model. Up to now, some reliable, higher-order accurate numerical methods have been constructed to solve the nonlinear Dirac equation (1.1). They include Crank-Nicholson type schemes [3,4], split-step spectral schemes [12], Legendre rational spectral methods [23], adaptive mesh method [22], and Runge-Kutta discontinuous Galerkin (RKDG) methods [17], etc. The interaction dynamics for the solitary wave solutions of (1.1) were numerically simulated in [4] by using a second-order accurate difference scheme. The authors saw there: charge and energy interchange except for some particular initial velocities of the solitary waves; inelastic interaction in binary collisions; and bound state production from binary collisions. Weakly inelastic interaction in ternary collisions is observed in [17]. The interaction dynamics in the binary and ternary collisions of two-humped solitary waves were first investigated in [18].

However, the experiments carried out in the literatures are all limited to the binary and ternary collisions of in-phase solitary waves of (1.1). In fact, the relative phase of those waves may vary with the interaction (see **Case B1** in Section 3), and their interaction generally depends on the initial phase shift. In this paper we will devote ourselves to further investigating the interaction dynamics in the binary and ternary collisions of the Dirac solitary waves with an initial phase shift by using the fourth-order accurate RKDG method [17] and the phase plane method, and report some interesting observations. The phase plane method [1] is based on the analysis of solitary wave trajectories on the phase plane. The RKDG methods for the Soler model adopt a discontinuous piecewise polynomial space for the approximate solutions and the test functions, and an explicit, high-order Runge-Kutta time discretization [9–11, 17]. Various experiments in [17, 18] have demonstrated that the fourth-order RKDG method is numerically stable without generating numerical oscillation within a very long time interval, has uniformly numerical convergence-rates, and preserves conservation of the energy and charge.

The paper is organized as follows. We introduce the (1+1)-dimensional space-time version of the NLD model (1.1) as well as its two solitary wave solutions in Section 2, and

corresponding RKDG discretization in Section 3, respectively. Numerical experiments are conducted in Section 4 to investigate the interaction dynamics of two or three colliding Dirac solitary waves with a phase shift. Several concluding remarks are given in Section 5.

2 Preliminaries

We restrict our attention to the (1+1)-dimensional Soler model (1.1), which can be rewritten in a general form

$$\begin{cases} \partial_t \psi_1 + \partial_x \psi_2 + im\psi_1 + 2i\lambda f(|\psi_1|^2, |\psi_2|^2)\psi_1 = 0, \\ \partial_t \psi_2 + \partial_x \psi_1 - im\psi_2 + 2i\lambda g(|\psi_1|^2, |\psi_2|^2)\psi_2 = 0, \end{cases} \tag{2.1}$$

where $\psi_1(x,t)$ and $\psi_2(x,t)$ are two components of the spinor $\boldsymbol{\psi}(x,t)$, and $f(u,v)$ and $g(u,v)$ denote two nonlinear real functions, i.e.,

$$f = |\psi_2|^2 - |\psi_1|^2, \quad g = |\psi_1|^2 - |\psi_2|^2.$$

A standing wave solution of the above model is given as

$$\boldsymbol{\psi}^{sw}(x,t) \equiv \begin{pmatrix} \psi_1^{sw}(x,t) \\ \psi_2^{sw}(x,t) \end{pmatrix} = \begin{pmatrix} A(x) \\ iB(x) \end{pmatrix} e^{-i\Lambda t}, \quad 0 < \Lambda \leq m, \tag{2.2}$$

where

$$A(x) = \frac{\sqrt{\frac{1}{\lambda}(m^2 - \Lambda^2)(m + \Lambda) \cosh(x\sqrt{m^2 - \Lambda^2})}}{m + \Lambda \cosh(2x\sqrt{m^2 - \Lambda^2})}, \tag{2.3}$$

$$B(x) = \frac{\sqrt{\frac{1}{\lambda}(m^2 - \Lambda^2)(m - \Lambda) \sinh(x\sqrt{m^2 - \Lambda^2})}}{m + \Lambda \cosh(2x\sqrt{m^2 - \Lambda^2})}. \tag{2.4}$$

The system (1.1) also has a single solitary wave solution placed initially at x_0 with a velocity v :

$$\boldsymbol{\psi}^{ss}(x - x_0, t) = (\psi_1^{ss}(x - x_0, t), \psi_2^{ss}(x - x_0, t))^T, \tag{2.5}$$

where

$$\psi_1^{ss}(x - x_0, t) = \sqrt{\frac{\gamma + 1}{2}} \psi_1^{sw}(\tilde{x}, \tilde{t}) + \text{sign}(v) \sqrt{\frac{\gamma - 1}{2}} \psi_2^{sw}(\tilde{x}, \tilde{t}), \tag{2.6}$$

$$\psi_2^{ss}(x - x_0, t) = \sqrt{\frac{\gamma + 1}{2}} \psi_2^{sw}(\tilde{x}, \tilde{t}) + \text{sign}(v) \sqrt{\frac{\gamma - 1}{2}} \psi_1^{sw}(\tilde{x}, \tilde{t}). \tag{2.7}$$

Here $\gamma = 1/\sqrt{1 - v^2}$, $\tilde{x} = \gamma(x - x_0 - vt)$, $\tilde{t} = \gamma(t - v(x - x_0))$, ψ_1^{sw} and ψ_2^{sw} are defined in (2.2) and $\text{sign}(x)$ is the sign function, which returns 1 if $x > 0$, 0 if $x = 0$, and -1 if $x < 0$.

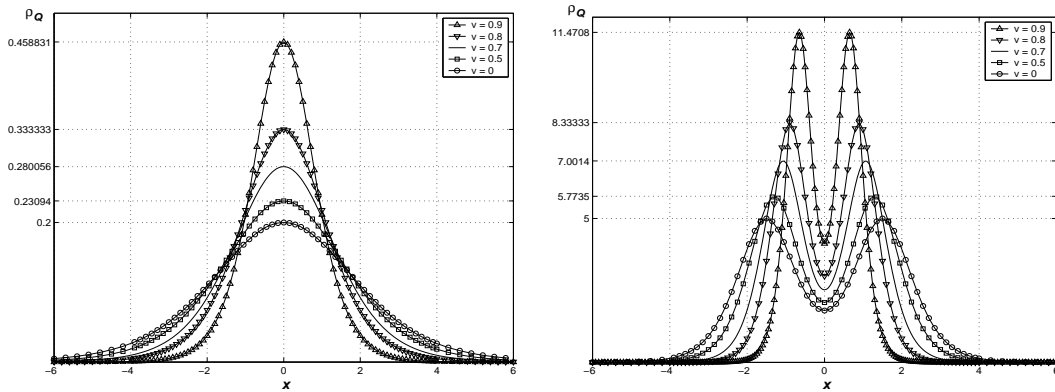


Figure 1: Dependence of ρ_Q on Λ and v . Left: $\Lambda=0.9$; right: $\Lambda=0.1$.

The function $\psi^{ss}(x-x_0, t)$ represents a solitary wave traveling from left to right if $v > 0$, or traveling from right to left if $v < 0$, and the standing wave $\psi^{sw}(x-x_0, t)$ is actually a solitary wave at rest placed at x_0 or identical to $\psi^{ss}(x-x_0, t)$ with $v=0$.

The profile of the solution (2.2) or (2.5) is strongly dependent on the parameter Λ : it is a two-humped solitary wave with two peaks whose locations are determined by

$$\cosh(2\sqrt{m^2 - \Lambda^2}\tilde{x}) = \frac{m^2 - \Lambda^2}{m\Lambda} \quad \text{if } 0 < \Lambda < \frac{m}{2};$$

it becomes a one-humped solitary wave with one peak located at $\tilde{x}=0$ if $\frac{m}{2} \leq \Lambda < m$; and $\psi^{ss}(x-x_0, t) \equiv 0$ if $\Lambda = m$. Moreover, the amplitude of the solitary waves also depends strongly on the velocity v :

$$\rho_Q^{ss}(x-x_0, t) = \gamma \rho_Q^{sw}(\tilde{x}, \tilde{t}).$$

Fig. 1 shows that dependence, which will give different interaction dynamics, where $\rho_Q(x, t)$ denotes the charge density and is defined by

$$\rho_Q(x, t) = |\psi_1|^2 + |\psi_2|^2. \tag{2.8}$$

It is worth noting that $e^{i\theta} \psi^{ss}(x-x_0, t)$ is still a solitary wave solution of the Soler model (1.1), if θ is a constant.

3 Numerical schemes

For completeness, this section introduces the higher-order accurate RKDG methods approximating Eq. (2.1).

3.1 DG spatial discretization

For any partition of the computational domain, $\{x_j, j \in \mathbb{Z}\}$, we set $I_{j+\frac{1}{2}} = (x_j, x_{j+1})$ for the finite element, $h_{j+\frac{1}{2}} = x_{j+1} - x_j$, and $x_{j+\frac{1}{2}} = \frac{1}{2}(x_{j+1} + x_j)$ for all $j \in \mathbb{Z}$.

Multiplying two equations in (2.1) by the arbitrary, complex-valued test functions ϕ_1 and ϕ_2 , whose real parts and imaginary parts all belong to the finite element space \mathcal{V}_h^q , integrating them over the finite element $I_{j+\frac{1}{2}}$, $j \in \mathbb{Z}$, and replacing the exact solution ψ by its approximation $\psi_h = (\psi_{1,h}, \psi_{2,h})$, where the real part and the imaginary part of $\psi_{l,h}$ belong to \mathcal{V}_h^q too, $l=1,2$, we may derive by using a simple formal integration by parts as follows,

$$\int_{I_{j+\frac{1}{2}}} \phi_1 \frac{\partial \psi_{1,h}}{\partial t} dx + (\widehat{\psi}_2 \phi_1^-)_{j+1} - (\widehat{\psi}_2 \phi_1^+)_{j-1} - \int_{I_{j+\frac{1}{2}}} \psi_{2,h} \frac{\partial \phi_1}{\partial x} dx + \int_{I_{j+\frac{1}{2}}} i(m + 2\lambda f(|\psi_{1,h}|^2, |\psi_{2,h}|^2)) \psi_{1,h} \phi_1 dx = 0, \tag{3.1}$$

$$\int_{I_{j+\frac{1}{2}}} \phi_2 \frac{\partial \psi_{2,h}}{\partial t} dx + (\widehat{\psi}_1 \phi_2^-)_{j+1} - (\widehat{\psi}_1 \phi_2^+)_{j-1} - \int_{I_{j+\frac{1}{2}}} \psi_{1,h} \frac{\partial \phi_2}{\partial x} dx - \int_{I_{j+\frac{1}{2}}} i(m - 2\lambda g(|\psi_{1,h}|^2, |\psi_{2,h}|^2)) \psi_{2,h} \phi_2 dx = 0, \tag{3.2}$$

where

$$\mathcal{V}_h^q = \left\{ \phi \mid \phi(x) \in P^q(I_{j+\frac{1}{2}}) \text{ if } x \in I_{j+\frac{1}{2}}, \forall j \in \mathbb{Z} \right\}, \tag{3.3}$$

$P^q(I_{j+\frac{1}{2}})$ denotes the space of the real-valued polynomials on $I_{j+\frac{1}{2}}$ of degree at most q , $(\phi_i^+)_{j-1} = \phi_i(x_{j-1}+0)$, $(\phi_i^-)_{j+1} = \phi_i(x_{j+1}-0)$, and $(\widehat{\psi}_i)_j$ denotes an approximation of $\psi_{i,h}(x_j, t)$, $i=1,2$. Since the approximate solution $\psi_{i,h}(x_j, t)$ is discontinuous at the points x_j , $j \in \mathbb{Z}$, we must choose $(\widehat{\psi}_i)_j$ carefully in order to derive a stable scheme. Usually, $(\widehat{\psi}_i)_j$ is taken as a two-point numerical flux, which may be generally represented in the form

$$(\widehat{\psi}_i)_j := \widehat{h}_i(\psi_h(x_j-0, t), \psi_h(x_j+0, t)), \quad \widehat{h}_i(\psi, \psi) = \psi_i, \quad i=1,2.$$

In this work, we will restrict our attention to the upwind fluxes, which are defined by

$$(\widehat{\psi}_1)_j = \frac{1}{2}((\psi_1)_j^+ + (\psi_1)_j^- - (\psi_2)_j^+ + (\psi_2)_j^-), \tag{3.4}$$

$$(\widehat{\psi}_2)_j = \frac{1}{2}((\psi_2)_j^+ + (\psi_2)_j^- - (\psi_1)_j^+ + (\psi_1)_j^-), \tag{3.5}$$

where $(\psi_i)_j^+ = \psi_{i,h}(x_j+0, t)$, $(\psi_i)_j^- = \psi_{i,h}(x_j-0, t)$, $i=1,2$.

With such a choice of the numerical fluxes we can show that the semi-discrete DG method (3.1) and (3.2) for Eq. (2.1) satisfies the discrete l^2 -stability property [17].

For the actual numerical implementation, we decompose the complex function $\psi_i(x, t)$ into its real and imaginary parts by writing

$$\psi_i(x, t) = \psi_i^r(x, t) + i\psi_i^s(x, t), \quad i=1,2.$$

Under the new notations, the system (2.1) becomes

$$\begin{aligned} \partial_t \psi_1^r + \partial_x \psi_2^r - m \psi_1^s - 2\lambda f(|\psi_1|^2, |\psi_2|^2) \psi_1^s &= 0, \\ \partial_t \psi_1^s + \partial_x \psi_2^s + m \psi_1^r + 2\lambda f(|\psi_1|^2, |\psi_2|^2) \psi_1^r &= 0, \\ \partial_t \psi_2^r + \partial_x \psi_1^r + m \psi_2^s - 2\lambda g(|\psi_1|^2, |\psi_2|^2) \psi_2^s &= 0, \\ \partial_t \psi_2^s + \partial_x \psi_1^s - m \psi_2^r + 2\lambda g(|\psi_1|^2, |\psi_2|^2) \psi_2^r &= 0, \end{aligned}$$

and the discontinuous Galerkin method (3.1) and (3.2) becomes: find $\psi_i^r, \psi_i^s \in \mathcal{V}_h^q$, such that for all $\phi_1^r, \phi_1^s, \phi_2^r, \phi_2^s \in \mathcal{V}_h^q$.

$$\begin{aligned} \int_{I_{j+\frac{1}{2}}} \phi_1^r \partial_t \psi_1^r \, dx + (\widehat{\psi}_2^r \phi_1^{r,-})_{j+1} - (\widehat{\psi}_2^r \phi_1^{r,+})_j - \int_{I_{j+\frac{1}{2}}} \psi_2^r \partial_x \phi_1^r \, dx \\ - \int_{I_{j+\frac{1}{2}}} (m + 2\lambda f(|\psi_l|^2, |\psi_l|^2)) \psi_1^s \phi_1^r \, dx = 0, \end{aligned} \tag{3.6}$$

$$\begin{aligned} \int_{I_{j+\frac{1}{2}}} \phi_1^s \partial_t \psi_1^s \, dx + (\widehat{\psi}_2^s \phi_1^{s,-})_{j+1} - (\widehat{\psi}_2^s \phi_1^{s,+})_j - \int_{I_{j+\frac{1}{2}}} \psi_2^s \partial_x \phi_1^s \, dx \\ + \int_{I_{j+\frac{1}{2}}} (m + 2\lambda f(|\psi_l|^2, |\psi_l|^2)) \psi_1^r \phi_1^s \, dx = 0, \end{aligned} \tag{3.7}$$

$$\begin{aligned} \int_{I_{j+\frac{1}{2}}} \phi_2^r \partial_t \psi_2^r \, dx + (\widehat{\psi}_1^r \phi_2^{r,-})_{j+1} - (\widehat{\psi}_1^r \phi_2^{r,+})_j - \int_{I_{j+\frac{1}{2}}} \psi_1^r \partial_x \phi_2^r \, dx \\ + \int_{I_{j+\frac{1}{2}}} (m - 2\lambda g(|\psi_l|^2, |\psi_l|^2)) \psi_2^s \phi_2^r \, dx = 0, \end{aligned} \tag{3.8}$$

$$\begin{aligned} \int_{I_{j+\frac{1}{2}}} \phi_2^s \partial_t \psi_2^s \, dx + (\widehat{\psi}_1^s \phi_2^{s,-})_{j+1} - (\widehat{\psi}_1^s \phi_2^{s,+})_j - \int_{I_{j+\frac{1}{2}}} \psi_1^s \partial_x \phi_2^s \, dx \\ - \int_{I_{j+\frac{1}{2}}} (m - 2\lambda g(|\psi_l|^2, |\psi_l|^2)) \psi_2^r \phi_2^s \, dx = 0. \end{aligned} \tag{3.9}$$

Moreover, we will choose the Legendre polynomials $P_l(\xi)$ as local basis functions, and then we may exploit sufficiently their L^2 -orthogonality:

$$\int_{-1}^1 P_l(\xi) P_k(\xi) \, d\xi = \frac{2}{2l+1} \delta_{l,k}, \quad l \leq k, \tag{3.10}$$

to obtain a diagonal mass matrix so that we may construct an explicit discontinuous Galerkin method approximating the NLD equations. For $x \in \mathbb{R}$, we now express our approximation solution ψ_h as follows:

$$\psi_{i,h}^z(x,t) = \sum_{l=0}^q \psi_{i,j+\frac{1}{2}}^{z,(l)}(t) \phi_{i,j+\frac{1}{2}}^{z,(l)}(x) := \psi_{i,j+\frac{1}{2}}^z(x,t), \quad \text{if } x \in I_{j+\frac{1}{2}}, \tag{3.11}$$

where $i = 1, 2$, the superscript $z = r$ or s , and

$$\phi_{i,j+\frac{1}{2}}^{z,(l)}(x) = P_l(\tilde{\zeta}_{j+\frac{1}{2}}), \quad \tilde{\zeta}_{j+\frac{1}{2}} := \frac{2(x-x_{j+\frac{1}{2}})}{h_{j+\frac{1}{2}}}. \tag{3.12}$$

Then, using the local transformation $\tilde{\zeta}_{j+\frac{1}{2}}(x) = 2(x-x_{j+\frac{1}{2}})/h_{j+\frac{1}{2}}$ and the property of the Legendre polynomials that $P_l(1) = 1$ and $P_l(-1) = (-1)^l$, we may rewrite the weak formulation (3.6)-(3.9) in the simple form

$$\begin{aligned} &\left(\frac{h_{j+\frac{1}{2}}}{2l+1}\right) \frac{d}{dt} \psi_{1,j+\frac{1}{2}}^{r,(l)}(t) + \widehat{\psi}_{2,j+1}^r - (-1)^l \widehat{\psi}_{2,j}^r - \int_{I_{j+\frac{1}{2}}} \psi_{2,j+\frac{1}{2}}^r \partial_x \phi_{j+\frac{1}{2}}^{r,(l)}(x) dx \\ &\quad - \int_{I_{j+\frac{1}{2}}} (m+2\lambda f(|\psi_{1,j+\frac{1}{2}}|^2, |\psi_{2,j+\frac{1}{2}}|^2)) \psi_{1,j+\frac{1}{2}}^r(x,t) \phi_{j+\frac{1}{2}}^{r,(l)}(x) dx = 0, \end{aligned} \tag{3.13}$$

$$\begin{aligned} &\left(\frac{h_{j+\frac{1}{2}}}{2l+1}\right) \frac{d}{dt} \psi_{1,j+\frac{1}{2}}^{s,(l)}(t) + \widehat{\psi}_{2,j+1}^s - (-1)^l \widehat{\psi}_{2,j}^s - \int_{I_{j+\frac{1}{2}}} \psi_{2,j+\frac{1}{2}}^s \partial_x \phi_{j+\frac{1}{2}}^{s,(l)}(x) dx \\ &\quad + \int_{I_{j+\frac{1}{2}}} (m+2\lambda f(|\psi_{1,j+\frac{1}{2}}|^2, |\psi_{2,j+\frac{1}{2}}|^2)) \psi_{1,j+\frac{1}{2}}^s \phi_{j+\frac{1}{2}}^{s,(l)}(x) dx = 0, \end{aligned} \tag{3.14}$$

$$\begin{aligned} &\left(\frac{h_{j+\frac{1}{2}}}{2l+1}\right) \frac{d}{dt} \psi_{2,j+\frac{1}{2}}^{r,(l)}(t) + \widehat{\psi}_{1,j+1}^r - (-1)^l \widehat{\psi}_{1,j}^r - \int_{I_{j+\frac{1}{2}}} \psi_{1,j+\frac{1}{2}}^r \partial_x \phi_{j+\frac{1}{2}}^{r,(l)}(x) dx \\ &\quad + \int_{I_{j+\frac{1}{2}}} (m-2\lambda g(|\psi_{1,j+\frac{1}{2}}|^2, |\psi_{2,j+\frac{1}{2}}|^2)) \psi_{1,j+\frac{1}{2}}^r \phi_{j+\frac{1}{2}}^{r,(l)}(x) dx = 0, \end{aligned} \tag{3.15}$$

$$\begin{aligned} &\left(\frac{h_{j+\frac{1}{2}}}{2l+1}\right) \frac{d}{dt} \psi_{2,j+\frac{1}{2}}^{s,(l)}(t) + \widehat{\psi}_{1,j+1}^s - (-1)^l \widehat{\psi}_{1,j}^s - \int_{I_{j+\frac{1}{2}}} \psi_{1,j+\frac{1}{2}}^s \partial_x \phi_{j+\frac{1}{2}}^{s,(l)}(x) dx \\ &\quad - \int_{I_{j+\frac{1}{2}}} (m-2\lambda g(|\psi_{1,j+\frac{1}{2}}|^2, |\psi_{2,j+\frac{1}{2}}|^2)) \psi_{1,j+\frac{1}{2}}^s \phi_{j+\frac{1}{2}}^{s,(l)}(x) dx = 0, \end{aligned} \tag{3.16}$$

and calculate the initial degrees of freedom $\psi_{1,j+\frac{1}{2}}^{z,(l)}(0)$ as follows:

$$\psi_{1,j+\frac{1}{2}}^{z,(l)}(0) = \frac{2l+1}{h_{j+\frac{1}{2}}} \int_{I_{j+\frac{1}{2}}} \psi_1^z(x,0) \phi_{j+\frac{1}{2}}^{z,(l)}(x) dx, \tag{3.17}$$

$$\psi_{2,j+\frac{1}{2}}^{z,(l)}(0) = \frac{2l+1}{h_{j+\frac{1}{2}}} \int_{I_{j+\frac{1}{2}}} \psi_2^z(x,0) \phi_{j+\frac{1}{2}}^{z,(l)}(x) dx, \tag{3.18}$$

where $j \in \mathbb{Z}$ and $l = 0, \dots, q$. This shows that after discretizing in space by the DG method, we obtain a systems of ordinary differential equations (ODEs) for the degrees of freedom. The first integral term in each equation given in (3.13)-(3.16) can be computed exactly. As

an example, we give its value in (3.13) for the case of $q=3$, as follows:

$$\int_{I_{j+\frac{1}{2}}} \psi_{i,j+\frac{1}{2}}^z(x,t) \partial_x \phi_{j+\frac{1}{2}}^{z,(l)}(x) dx = \begin{cases} 0 & l=0, \\ 2\psi_{i,j+\frac{1}{2}}^{z,(0)}, & l=1, \\ 2\psi_{i,j+\frac{1}{2}}^{z,(1)}, & l=2, \\ 2(\psi_{i,j+\frac{1}{2}}^{z,(0)} + \psi_{i,j+\frac{1}{2}}^{z,(2)}), & l=3. \end{cases} \quad (3.19)$$

Other integrals will be computed numerically, e.g., by using Gaussian quadrature.

3.2 Time discretization

To discretize the ODE system (3.13)-(3.16) with the initial data (3.17)-(3.18), we use the higher-order Runge-Kutta time discretizations. As shown by Cockburn in [9], when the polynomials of degree q are used, a Runge-Kutta method of order $(q+1)$ must be used in order to guarantee that the scheme is stable. In this paper we use a fourth-order non-TVD Runge-Kutta scheme [19].

If a system of the ODEs is given in a compact form $\frac{d}{dt}U(t) = L(U)$, the fourth-order non-TVD Runge-Kutta scheme is given as

$$\begin{aligned} U^{(1)} &= U^n + \frac{1}{2}\Delta t L(U^n), \\ U^{(2)} &= U^n + \frac{1}{2}\Delta t L(U^{(1)}), \\ U^{(3)} &= U^n + \Delta t L(U^{(2)}), \\ U^{n+1} &= \frac{1}{3} \left(U^{(1)} + 2U^{(2)} + U^{(3)} - U^n + \frac{1}{2}\Delta t L(U^{(3)}) \right). \end{aligned} \quad (3.20)$$

4 Numerical experiments

This section gives numerical experiments on the interaction of two or three colliding Dirac solitary waves with a phase shift. Our computations will work in dimensionless units, or equivalently, take $m=1$ and $\lambda=\frac{1}{2}$, and adopt the non-reflecting boundary conditions at two boundaries of the computational domain. The domain is covered by some identical cells with area of 0.05. The initial conditions are created in the form of superposition of two or three isolated solitary waves defined in (2.5).

4.1 Binary collisions

This subsection solves the Soler model (1.1) with the initial data

$$\psi(x,0) = e^{i\theta_l} \psi^{ss}(x-x_l,0) + e^{i\theta_r} \psi^{ss}(x-x_r,0), \quad (4.1)$$

where θ_l and θ_r are two real numbers, determining the initial phases of corresponding waves. For convenience, two solitary waves are said to be equal if $\Lambda_l = \Lambda_r$ and $|v_l| = |v_r|$, and we denote by $r(t)$ and $\theta(t)$ the separation and the relative phase between solitary waves, respectively, especially, $r(0) = x_r - x_l$ and $\theta(0) = \theta_r - \theta_l$.

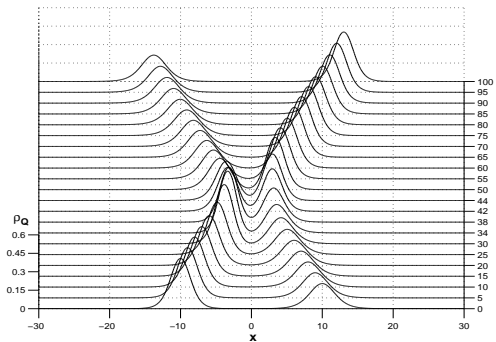


Figure 2: **Case B1.** The time evolution of the charge density ρ_Q . $\Lambda_l = 0.8, \Lambda_r = 0.9, v_l = -v_r = 0.2, \theta(0) = 0, x_r = -x_l = 10$.

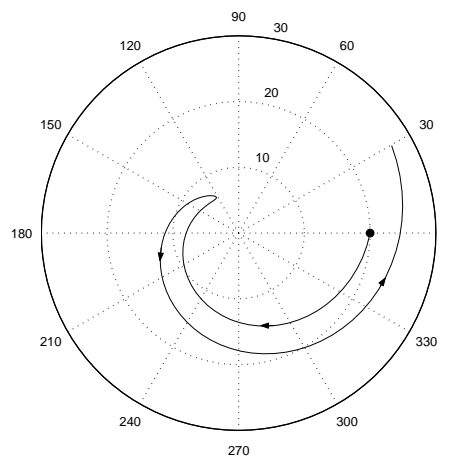


Figure 3: **Case B1.** The solitary wave interaction trajectory in the (r, θ) plane.

4.1.1 Two one-humped solitary waves

Case B1. The first experiment is conducted to reveal that the relative phase of Dirac solitary waves may change with the interaction. The parameters in (4.1) are taken as $\Lambda_l = 0.8, \Lambda_r = 0.9, v_l = -v_r = 0.2, \theta_l = \theta_r = 0$, and $x_r = -x_l = 10$. It means that two initial waves are unequal, but in-phase and one-humped. Fig. 2 shows the time evolution of the charge density ρ_Q . No overlap happens there. In order to investigate the time evolution of the relative phase $\theta(t)$ in binary collisions, corresponding solitary wave interaction trajectory on the (r, θ) plane is drawn in Fig. 3, where the big black dots denote the initial positions of the solitary waves in the phase plane, and the arrows represent the motion

directions. The phase plane plot further demonstrates the above observation because of the positive separation $r(t)$ for all $t \geq 0$, and shows that the relative phase of Dirac solitary waves may vary with the interaction even though two initial waves are in-phase, and the relative phase $\theta(t)$ changes clockwise (anticlockwise) with respect to the time before (after) the interaction around $t = 42$. It is interesting to investigate the interaction dynamics of Dirac solitary waves with a phase shift.

Case B2. The second experiment is to investigate the interaction dynamics of two equal but initially motioning one-humped solitary waves with a phase shift. Some parameters in (4.1) are prescribed as $\Lambda_l = \Lambda_r = 0.5$, $v_l = -v_r = 0.2$, $\theta_l = 0$, and $x_r = -x_l = 10$. Figs. 4 and 5 show the charge densities for $\theta(0) = 0, \pi/4, 3\pi/4$, and π . It is seen that when $\theta(0) = \pi$, the elastic interaction happens and two solitary waves keep their initial shapes and velocities after their collisions, see the left plot of Fig. 4. In contrast, strong overlap happens when $\theta(0) = 0$, see the right plot of Fig. 4. In both cases ($\theta(0) = 0$ and π), the charge densities are always symmetric, but this property will be lost when $\theta(0) = \pi/4$ and $3\pi/4$, see Fig. 5.

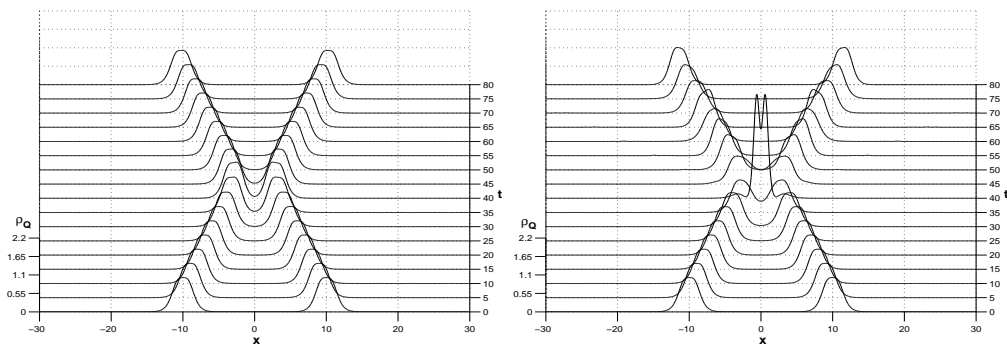


Figure 4: **Case B2.** The time evolution of the charge density ρ_Q . $\Lambda_l = \Lambda_r = 0.5$, $v_l = -v_r = 0.2$, $\theta_l = 0$, $x_r = -x_l = 10$. Left: $\theta_r = \pi$, right: $\theta_r = 0$.

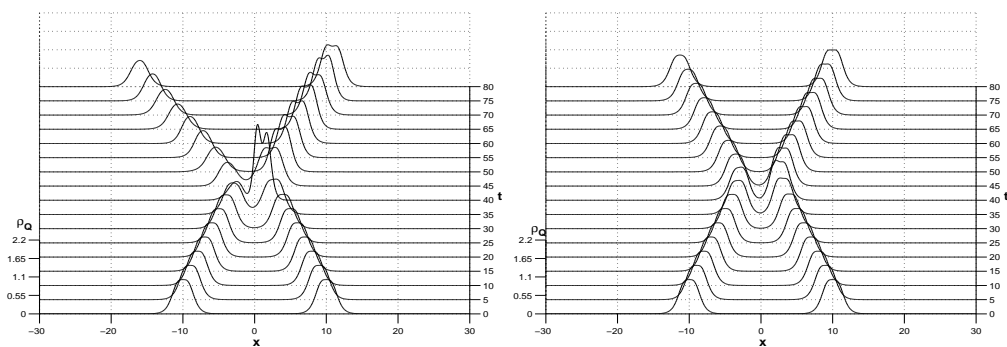


Figure 5: Same as Fig. 4 except for different θ_r . Left: $\theta_r = \pi/4$; right: $\theta_r = 3\pi/4$.

The solitary wave interaction trajectories in the (r, θ) plane in Fig. 6 show that if two solitary waves are in-phase and equal initially, they will be also in-phase during the inter-

action and may fully overlap each other because $r(t)$ may be equal to zero; if two equal waves are out-of-phase initially, so are they during the interaction, but the overlap does not happen because $r(t)$ is always bigger than zero; if the initial phase shift is equal to $\pi/4$, $\pi/2$, or $3\pi/4$, the overlap does not appear too, and the relative phase varies periodically after the collision and anticlockwise. Moreover, when $\theta(0)$ increases, the minimum separation increases too. Generally, the relative phase of 0 and π are two limiting cases in which the corresponding interaction dynamics is the “strongest”. The interaction dynamics will vary continuously from a limiting case to another as the initial relative phase $\theta(0)$ is taken over the domain $[0, \pi]$.

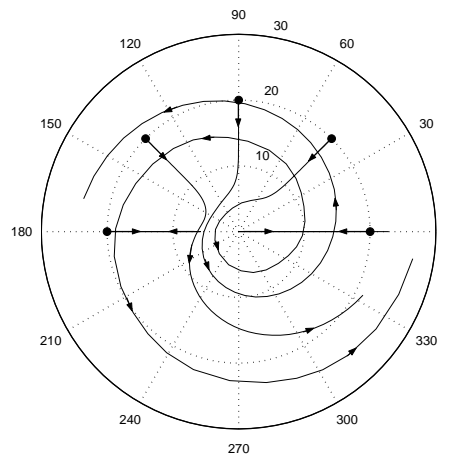


Figure 6: **Case B2.** The solitary wave interaction trajectories in the (r, θ) plane.

Case B3. The third experiment is to investigate the interaction dynamics of two equal but initially resting one-humped solitary waves with a phase shift. We take $\Lambda_l = \Lambda_r = 0.6$, and $x_r = -x_l = 3$. The charge density for the case of $\theta(0) = 0$ has been given in Fig. 3 of [17], which was showing a long-lived oscillating bound state. When $\theta(0) = \pi$, it is seen from Fig. 7 that two waves repulse fully each other. So the interaction of two out-of-phase waves are fully different from that of two in-phase waves. Fig. 8 depicts the solitary wave interaction trajectories on the (r, θ) plane for five initial phase shifts, i.e., $\theta(0) = 0, \pi/4, \pi/2, 3\pi/4, \pi$. Those results further demonstrate the above observation, and show that the relative phase varies periodically during the whole interaction and anticlockwise. Similar to the above case, when $\theta(0) = 0$ and π , $\theta(t)$ keeps corresponding constant. Notice that no arrow is added to the trajectory for $\theta(0) = 0$ due to the oscillating state.

It is worth mentioning that we have conducted various different experiments on binary collisions of one-humped waves and can conclude that collapse phenomena cannot be generally observed in collisions between two one-humped waves. The interaction trajectories in the (r, θ) plane can be obtained and are similar to those in Figs. 5 and 8. To save space, corresponding plots are not given here.

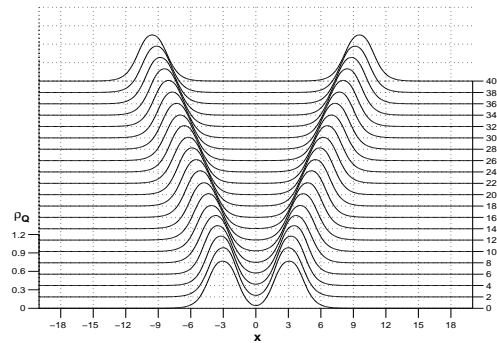


Figure 7: **Case B3.** The time evolution of the charge density ρ_Q for two initially resting, equal waves. $\Lambda_l = \Lambda_r = 0.6$, $x_r = -x_l = 3$, $\theta(0) = \pi$.

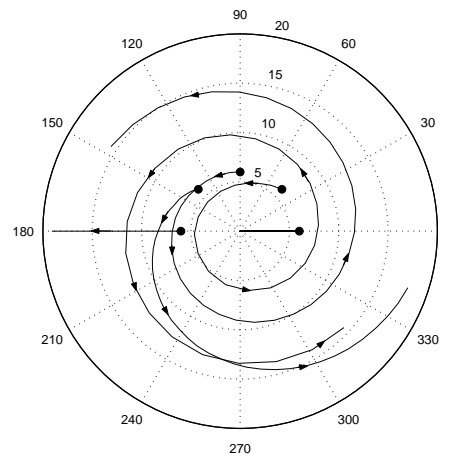


Figure 8: **Case B3.** The solitary wave interaction trajectories in the (r, θ) plane.

4.1.2 Two two-humped solitary waves

Here we study the interaction of two two-humped solitary waves with a phase shift.

Case B4. This case studies the interaction of two equal and initially motioning two-humped waves and takes $\Lambda_l = \Lambda_r = 0.1$, $v_l = -v_r = 0.2$, and $x_r = -x_l = 10$. The computed charge density for two initially out-of-phase solitary waves presented in Fig. 9 shows that the final solitary waves keep their initial velocities but with slightly different shapes; collapse does not happen in this case. However, as shown in Fig. 2 in [18], the collapse will happen if those two waves are in-phase initially. Fig. 10 gives the interaction trajectories on the (r, θ) plane for three initial phase shifts, i.e., $\theta(0) = \pi/2, 3\pi/4, \pi$. The results show that the relative phase is always π and no overlap happens if the two initial waves are out-of-phase. For the other two cases, the relative phase varies periodically after the collision and anticlockwise. By the way, the above phase plane approach is not very suitable for the case in which the waves collapse or are always oscillating during the interaction.

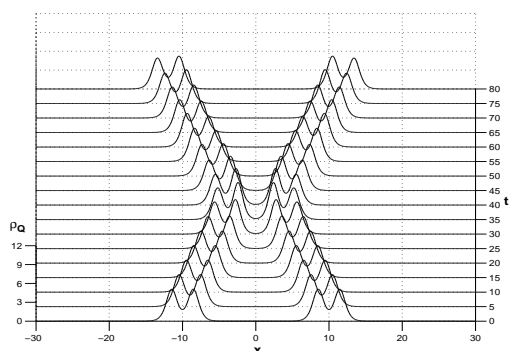


Figure 9: **Case B4**. The time evolution of the charge density ρ_Q . $\Lambda_l = \Lambda_r = 0.1$, $x_r = -x_l = 10$, $v_l = -v_r = 0.2$, $\theta(0) = \pi$.

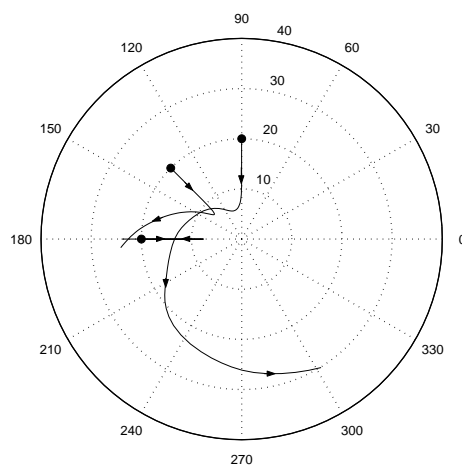


Figure 10: **Case B4**. The solitary wave interaction trajectories in the (r, θ) plane.

Case B5. This experiment considers the interaction of two unequal and initially resting two-humped waves with a phase shift of π . The results given in Fig. 11 show that they repulse each other essentially, and the repulsion force depends on their initial separation. When two initial waves stand more nearly, the repulsion dominates in their interaction, thus they move outside fast and cannot re-collide each other, see the left figure in Fig. 11. But when the separation is relatively big, the right plot of Fig. 11 shows that two waves first repulse each other, then attract afterwards and collapse. When two initial waves are equal, at rest, and with a phase shift of π , we only observe full repulsion which is similar to that in the left figure of Fig. 11.

Various experiments tell us that collapse happens easily in collisions of two in-phase, equal, two-humped waves, but it may not appear in collisions between two in-phase, unequal, two-humped waves, or two two-humped waves with a phase shift of π .

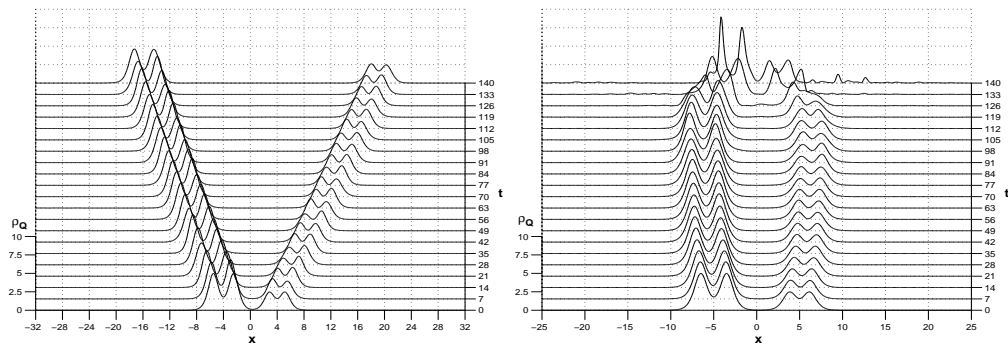


Figure 11: **Case B5.** The time evolution of the charge density ρ_Q for two initially resting waves. $\Lambda_l=0.1, \Lambda_r=0.2$, $\theta(0) = \pi$. Left: $x_r = -x_l = 4$; right: $x_r = -x_l = 5$.

4.1.3 A one-humped solitary wave and a two-humped solitary wave

In the following we study the interaction of a one-humped solitary wave and a two-humped solitary wave, which are with a phase shift of π .

Case B6. Fig. 12 shows the computed results for the case of $\Lambda_l=0.1, \Lambda_r=0.9$, $v_l = -v_r = 0$, and $x_r = -x_l = 6$. We see the quasi-stable long-lived oscillating bound state, which is essentially same as one shown in Fig. 3 in the paper [18]. Generally, when there is a big difference between the peak values of two initial waves, macroscopical behavior of the interaction dynamics is essentially independent on their initial phase shift.

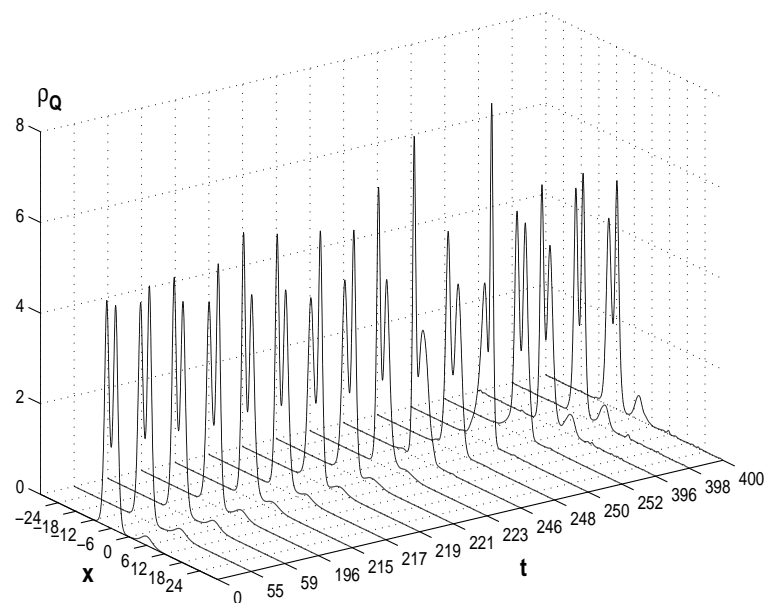


Figure 12: **Case B6.** Bound state formed in binary collisions between two initially resting, out-of-phase waves. $\Lambda_l=0.1, \Lambda_r=0.9$, $v_l = v_r = 0$, $x_r = -x_l = 6$, $\theta(0) = \pi$.

Case B7. Fig. 13 shows the computed results for the cases of $\Lambda_l = 0.1, \Lambda_r = 0.5$ and 0.9 , $v_l = -v_r = 0.2$, $\theta(0) = \pi$, and $x_r = -x_l = 10$. It tells us that collapse may be observed in collisions between a one-humped solitary wave and a two-humped solitary wave when they do initially travel face to face, but it may also not happen.

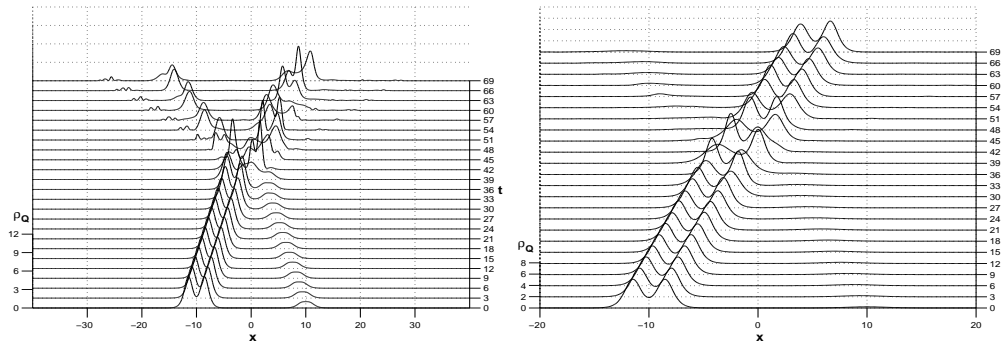


Figure 13: **Case B7.** The time evolution of the charge density ρ_Q . $\Lambda_l = 0.1$, $v_l = -v_r = 0.2$, $x_r = -x_l = 10$, $\theta(0) = \pi$. Left: $\Lambda_r = 0.5$; right: $\Lambda_r = 0.9$.

4.2 Ternary collisions

In this subsection, we study ternary collisions by solving the nonlinear Dirac model (1.1) with the following initial data

$$\psi(x,0) = e^{i\theta_l} \psi_l^{ss}(x-x_l,0) + e^{i\theta_m} \psi_m^{ss}(x-x_m,0) + e^{i\theta_r} \psi_r^{ss}(x-x_r,0), \tag{4.2}$$

where θ_l, θ_m and θ_r are three real numbers, determining the initial phases of corresponding waves.

Case T1. The first case we consider is collisions of three initially resting two-humped solitary waves: $\Lambda_l = \Lambda_m = \Lambda_r = 0.1$, $v_l = v_m = v_r = 0$, $x_r = -x_l = 10$, $x_m = 0$, $\theta_l = \theta_r = 0$, and $\theta_m = \pi$. The results are shown in Fig. 14. We see from the left plot that the waves first repulse each other because two neighboring waves are out-of-phase, but after $t = 100$ they begin to attract each other, and final collision results in collapse. Symmetry of the solutions is kept very well. The right figure of Fig. 14 gives the charge and energy densities at $x = 0$ as a function of time, $\rho_E(0,t)$ and $\rho_Q(0,t)$, where the energy density $\rho_E(x,t)$ is defined by

$$\rho_E(x,t) = \text{Im}(\psi_1^* \partial_x \psi_2 + \psi_2^* \partial_x \psi_1) + m(|\psi_1|^2 - |\psi_2|^2) - \lambda(|\psi_1|^2 - |\psi_2|^2)^2. \tag{4.3}$$

We observe that before collapse happens, the middle wave is oscillating because of bind from left and right waves although its displacement seems to be unchanged.

Case T2. The second case is collisions of three initially resting one-humped waves: $\Lambda_l = \Lambda_m = \Lambda_r = 0.5$, $v_l = v_m = v_r = 0$, $x_r = -x_l = 10$, $x_m = 0$, $\theta_l = \pi$, and $\theta_m = \theta_r = 0$. The results are shown in the left plot of Fig. 15. It is seen that the first collision happens between two right in-phase waves around $t = 45$, and then two faster moving waves are formed.

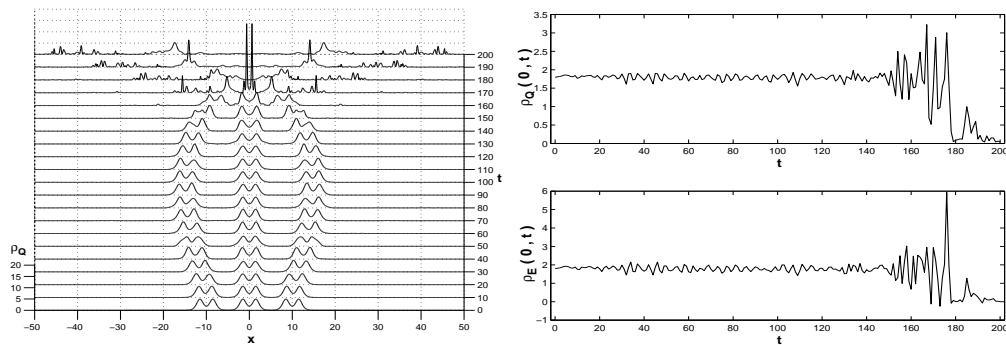


Figure 14: **Case T1.** Collisions of three initially resting two-humped waves: $\Lambda_l = \Lambda_m = \Lambda_r = 0.1$, $x_r = -x_l = 10$, $x_m = 0$, $\theta_l = \theta_r = 0$, $\theta_m = \pi$. Left: plot of $\rho_Q(x,t)$; right: plots of $\rho_Q(0,t)$ and $\rho_E(0,t)$.

The initially resting left wave begin to be moving towards left due to repulsion between it and the right waves, and then it is caught up with and interacted by the left moving wave generated in the first collision around $t = 113$. Overlapping happens in all two collisions. If we consider collisions of three initially resting one-humped waves with $\Lambda_l = \Lambda_m = \Lambda_r = 0.6$ or 0.9 , the interaction does only happen between two right neighboring in-phase waves, see the right plot of Fig. 15. The reason is that the left-moving (middle) wave formed in the interaction of two initially in-phase (right) waves is not faster than the left wave.

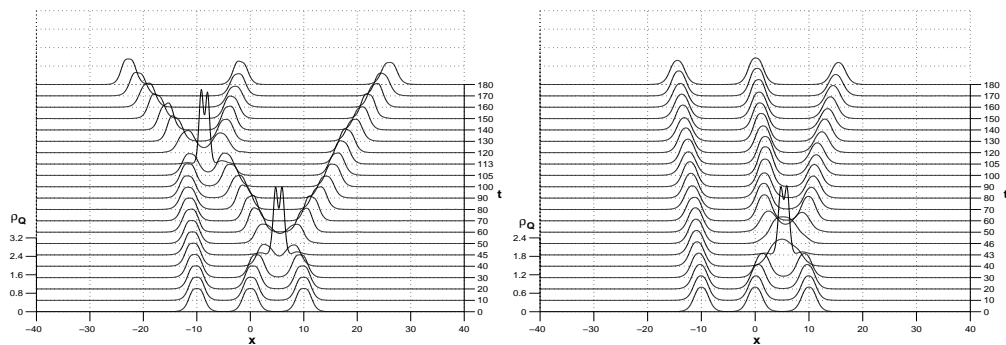


Figure 15: **Case T2.** The time evolution of the charge density ρ_Q . $v_l = v_m = v_r = 0$, $x_r = -x_l = 10$, $x_m = 0$, $\theta_l = \pi$, $\theta_m = \theta_r = 0$. Left: $\Lambda_l = \Lambda_m = \Lambda_r = 0.5$; right: $\Lambda_l = \Lambda_m = \Lambda_r = 0.6$.

5 Discussions and conclusions

This paper has further studied the interaction dynamics for solitary waves of the Soler model (1.1) by using the fourth-order accurate Runge-Kutta discontinuous Galerkin method [17, 18] and the phase plane method which was employed for the first time to analyze the interaction of Dirac waves.

From our experiments on the interaction of Dirac solitary waves with an initial phase shift, we observed the following new phenomena: (a) full repulsion in binary and ternary collisions, and the initial distance between waves is smaller the repulsion is stronger; (b) repulsing first, attracting afterwards, and then collapse in binary and ternary collisions of two-humped waves; (c) interaction with one overlap and two overlaps in ternary collisions of initially resting waves, which depends on initial parameter Λ . Moreover, the collapse phenomenon cannot be observed in collisions between one-humped waves generally, but it happens easily in collisions of in-phase, equal, two-humped waves; the macroscopical behavior of the interaction dynamics is essentially independent on their initial phase shift, when there is a big difference between the peak values of the initial waves.

The phase plane method can show the evolution of the relative phase of the solitary waves during their collisions. In this paper, it was used to further demonstrate some of the experiment phenomena, and reveal the fact that the relative phase of Dirac solitary waves may vary with the interaction. Generally, the interaction of Dirac solitary waves for the Soler model depends on the relative phase between them: if two equal solitary waves are in-phase or out-of-phase initially, so are they during the interaction; if the initial phase shift is far away from 0 and π , the relative phase begins to periodically vary after a finite time.

Acknowledgments

This research was partially supported by the National Basic Research Program under the Grant 2005CB321703, NCET and the National Natural Science Foundation of China (No. 10431050, 10576001).

References

- [1] V. V. Afanasjev and N. Akhmediev, Soliton interaction in nonequilibrium dynamical systems, *Phys. Rev. E*, 53 (1996), 6471-6475.
- [2] A. Alvarez, Spinorial solitary wave dynamics of a (1+3)-dimensional model, *Phys. Rev. D*, 31 (1985), 2701-2703.
- [3] A. Alvarez, Linearized Crank-Nicholson scheme for nonlinear Dirac equations, *J. Comput. Phys.*, 99 (1992), 348-350.
- [4] A. Alvarez and B. Carreras, Interaction dynamics for the solitary waves of a nonlinear Dirac model, *Phys. Lett. A*, 86 (1981), 327-332.
- [5] A. Alvarez and A. F. Rañda, Blow-up in nonlinear models of extended particles with confined constituents, *Phys. Rev. D*, 38 (1988), 3330-3333.
- [6] A. Alvarez and M. Soler, Energetic stability criterion for a nonlinear spinorial model, *Phys. Rev. Lett.*, 50 (1983), 1230-1233.
- [7] A. Alvarez and M. Soler, Stability of the minimum solitary wave of a nonlinear spinorial model, *Phys. Rev. D*, 34 (1986), 644-645.

- [8] P. Blanchard, J. Stubbe and L. Vázquez, Stability of nonlinear spinor fields with application to the Gross-Neveu model, *Phys. Rev. D*, 36 (1987), 2422-2428.
- [9] B. Cockburn, Discontinuous Galerkin methods for convection-dominated problems, in: T. J. Barth and H. Deconinck (Eds.), *High-Order Methods for Computational Physics*, Lecture Notes in Computational Science and Engineering, Vol. 9, Springer, 1999, pp. 69-224.
- [10] B. Cockburn and C. W. Shu, TVB Runge-Kutta local projection discontinuous Galerkin finite element method for conservation laws II: General framework, *Math. Comput.*, 52 (1989), 411-435.
- [11] B. Cockburn, S. Y. Lin and C. W. Shu, TVB Runge-Kutta local projection discontinuous Galerkin finite element method for conservation laws III: One dimensional systems, *J. Comput. Phys.*, 84 (1989), 90-113.
- [12] J. De Frutos and J. M. Sanz-Serna, Split-step spectral schemes for nonlinear Dirac systems, *J. Comput. Phys.*, 83 (1989), 407-423.
- [13] M. J. Esteban and E. Séré, An overview on linear and nonlinear Dirac equations, *Discrete Cont. Dyn. Syst.*, 8 (2002), 381-397.
- [14] A. F. Rañada, Classical nonlinear Dirac field models of extended particles, in: A. O. Barut (Ed.), *Quantum Theory, Groups, Fields and Particles*, 1983, pp. 271-291.
- [15] A. F. Rañada, M. F. Rañada, M. Soler and L. Vázquez, Classical electrodynamics of a nonlinear Dirac field with anomalous magnetic moment, *Phys. Rev. D*, 10 (1974), 517-525.
- [16] A. F. Rañada and M. Soler, Perturbation theory for an exactly soluble spinor model in interaction with its electromagnetic field, *Phys. Rev. D*, 8 (1973), 3430-3433.
- [17] S. H. Shao and H. Z. Tang, Higher-order accurate Runge-Kutta discontinuous Galerkin methods for a nonlinear Dirac model, *Discrete Cont. Dyn.-B*, 6 (2006), 623-640.
- [18] S. H. Shao and H. Z. Tang, Interaction for the solitary waves of a nonlinear Dirac model, *Phys. Lett. A*, 345 (2005), 119-128.
- [19] C. W. Shu and S. Osher, Efficient implementation of essentially non-oscillatory shock-capturing schemes, *J. Comput. Phys.*, 77 (1988), 439-471.
- [20] M. Soler, Classical, stable, nonlinear spinor field with positive rest energy, *Phys. Rev. D*, 1 (1970), 2766-2769.
- [21] W. A. Strauss and L. Vázquez, Stability under dilations of nonlinear spinor field, *Phys. Rev. D*, 34 (1986), 641-643.
- [22] H. Wang and H. Z. Tang, An efficient adaptive mesh redistribution method for a nonlinear Dirac equation, *J. Comput. Phys.*, 222 (2007), 176-193.
- [23] Z. Q. Wang and B. Y. Guo, Modified Legendre rational spectral method for the whole line, *J. Comput. Math.*, 22 (2004), 457-474.